

Supplemental Information for:

Influence of temperature on the differential capacitance of ionic liquid electrolytes on charged surfaces.

Jenel Vatamanu^{*a}, Lidan Xing^b, Weishan Li^b, Dmitry Bedrov^a

a) Department of Materials Science and Engineering, University of Utah, 122 South Central Campus Drive, Salt Lake City, Utah 84112, United States

b) School of Chemistry and Environment, South China Normal University, Guangzhou 510006, China

*u0615401@utah.edu

Table 1. Technical details about the MD simulations utilized in this work.

Electrode Material /number of atoms	Electrolyte / ionic pairs	Potential difference between two electrodes (V)	Trajectory lengths (ns)	T(K)	Box sizes (Å)/cross-section area (System periodicity)
Flat surface (S1)					
Flat / 480 atoms	pyr13/FSI (190 ionic pairs)	0.0, 0.2, 0.4, 0.6, 0.8, 1.0, 1.2, 1.6, 2.0, 2.4, 2.8, 3.2, 3.6, 4.0, 4.4, 5.0	50ns	363, 533	25.61x24.65 (2D*)
Prismatic graphite (S2)					
Prismatic / 320 atoms	pyr13/FSI (190 ionic pairs)	0.0, 0.2, 0.3, 0.4, 0.6, 0.8, 1.0, 1.2, 1.6, 2.0, 2.4, 2.8, 3.2, 3.6, 4.0, 4.4	50ns	363, 533	24.65x26.80 (2D)
Weak roughness model (S3)					
Rough surface / 720 atoms	pyr13/FSI (466 ionic pairs)	0.0, 0.2, 0.3, 0.4, 0.6, 0.8, 1.0, 1.2, 1.6, 2.0, 2.4, 2.8, 3.2, 3.6, 4.0, 4.4	50ns	363, 463, 533	29.57x40.20 (2D)
Strong roughness model (S4)					
Rough surface / 840 atoms	pyr13/FSI (466 ionic pairs)	0.0, 0.1, 0.2, 0.3, 0.4, 0.5, 0.6, 0.7, 0.8, 0.9, 1.0, 1.1, 1.2, 1.4, 1.6, 1.8, 2.0, 2.2, 2.4, 2.6, 2.8, 3.2, 3.6, 4.0, 4.4	50 ns	363	34.50x36.50 (2D)
Rough surface / 840 atoms	pyr13/FSI (466 ionic pairs)	0.0, 0.2, 0.3, 0.4, 0.6, 0.8, 1.0, 1.2, 1.6, 1.8, 2.0, 2.4, 2.8, 3.2, 3.6, 4.0, 4.3	25 ns	393	34.50x36.50 (2D)
Rough surface / 840 atoms	pyr13/FSI (466 ionic pairs)	0.0, 0.2, 0.3, 0.4, 0.6, 0.8, 1.0, 1.2, 1.6, 1.8, 2.0, 2.4, 2.8, 3.2, 3.6, 4.0, 4.4	50 ns	463, 533	34.50x36.50 (2D)

*For the 2D geometry systems the direction of asymmetry was our z-axis. Therefore the size of simulation box along z-axis is not important for 2D geometry because we don't employ periodicity along z-direction. Note that selected trajectories were re-run from different initial conditions. The distance between electrodes varied between 118 to 150Å depending on surface type and temperature.

To ensure convergence of the simulation data and properties extracted from simulations we have conducted an extensive analysis of the error bars for the key properties (density profiles across the simulation box, interfacial composition, electrode capacity) utilizing the procedure described in our previous work.¹ As the closely spaced points along the trajectory are correlated, we grouped the simulation data into consecutive blocks with increasing block size until consecutive blocks become uncorrelated following the block average methodology described in the Appendix D of Frenkel and Smit bookⁱⁱ. Dividing a typical trajectory of 25 ns into 100 - 250 blocks we found that for an 80% confidence interval the error bars in bulk density profiles are less than 1.5%. Although, right at the interface, the error bars tend to increase for co-ions, this is less important because the concentration of co-ions is small in absolute value near the surface (as the voltage increases). However, the overall noise in the electrode capacitance can be larger than what one would expect to get from the integration and subsequent differentiation of density profiles with 1.5% error bars due to other errors such as e.g. the uncertainty of numerical derivatives discussed below.

When we compute differential capacitance using numerical derivatives of charge vs potential data we use several consecutive points (typically 5) and first do local fit of the selected points with parabolic function. Then a derivative in the central point is determined analytically from the fit parabola. This procedure, conducted for all combination of consecutive points, results in implicit smoothing of the noise in the raw data and therefore allows better accuracy in determining capacitance.

Therefore as long as we are confident that ions distribution density profiles and hence the resulting electrode charge vs potential are converged during simulation, the properties obtained using derivatives should also have a good convergence. To insure the former, for selected systems and potentials we conducted simulations that have two to four times longer trajectories than the standard estimated time required for convergence as well as run additional trajectories starting from independent initial conditions. In all of those simulations we did not see any significant variations between the data (see below).

Several selected trajectories were duplicated from different initial conditions. The reproducibility of our results is illustrated in Fig 1 below where the data for electrode charge density vs potential ($\sigma=f(U)$) are compared for the two systems with atomically rough surfaces. For each system two independent trajectories were run of different length. As we can see both trajectories produced basically identical dependencies (red vs. black lines $\sigma=f(U)$) indicating the reproducibility of our results. Note that much shorter trajectories can be sufficient to capture the trend.

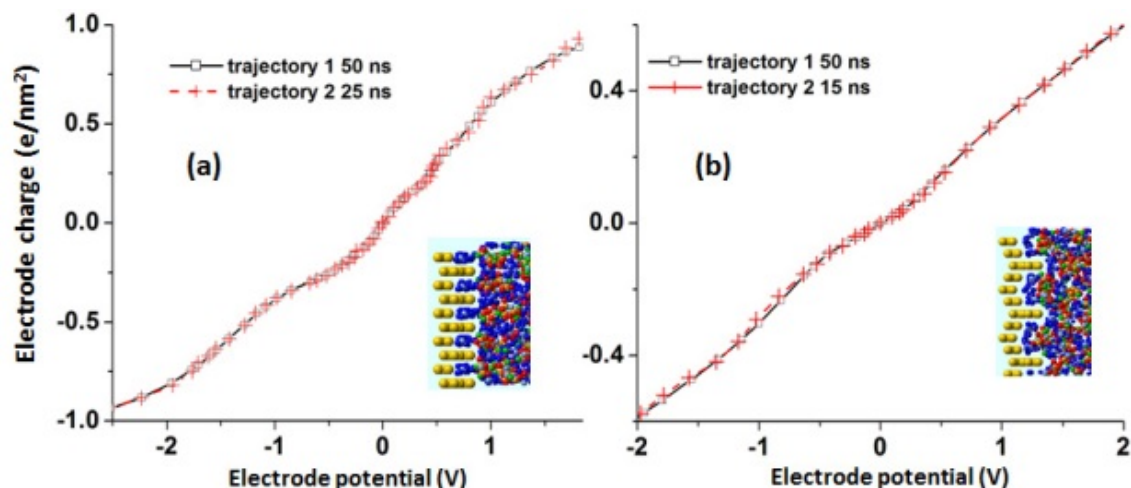


Figure 1.

A comparison for the electrode charge vs. electrode potential for two independent trajectories and for 2 different systems at 363K. Note that the lengths of trajectories were different (15, 25 and 50ns), yet they produced virtually identical results for the electrode charge. The agreement between the red and the black lines/symbols prove the reproducibility of our results.

However, we are focusing on the properties that are defined by numerical derivatives of the data plotted in Figure 1. To illustrate that our derivation protocol (described above) combine with the amount of collected statistics result in accurate and converged data for the differential capacitance Figure 2 compares the DC obtained from 12.5ns blocks of a 50ns run for the system shown in Figure 1a.

Therefore, we are confident that our simulations are run long enough that all key relaxation processes (ion rearrangement in the EDL, ions exchange between EDL and the bulk, bulk diffusion of ions, etc.) have been accessed by the system over simulation time even at large potentials where the interfacial layer can be very lethargic.

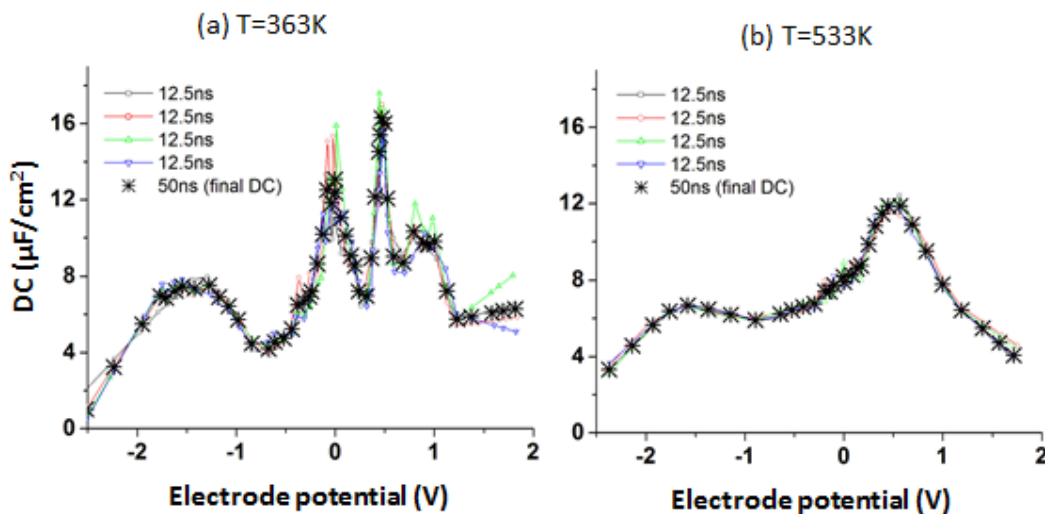


Figure 2.

Differential capacitance vs electrode potential for the system shown in Fig 3a as obtained for four independent trajectory blocks as well as for the whole trajectory.

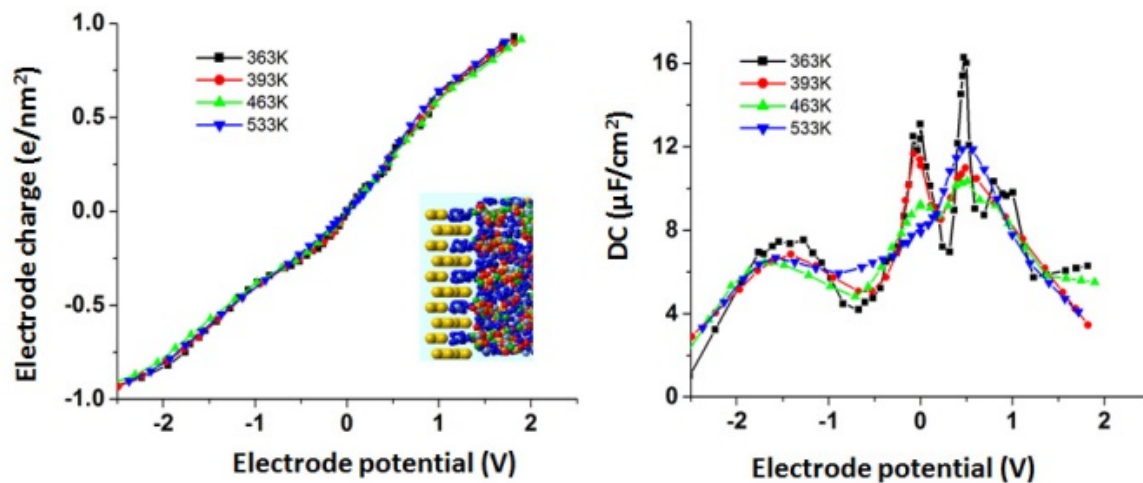


Figure 3.

The electrode surface charge density (left panel) and the corresponding DC (right panel) for the surface model S4 at various temperatures. An additional trajectory at 393K was added (red line). The data from 393K was not included in the main manuscript for clarity. Consistent with the trend already shown in the main manuscript, the DC at 393K is smoother (smaller oscillations between maxima and minima) than the DC at 363K. However the overall slope of electrode-charge vs. voltage (and the average value of DC) at 393K is very similar to that at 363K or at higher temperatures.

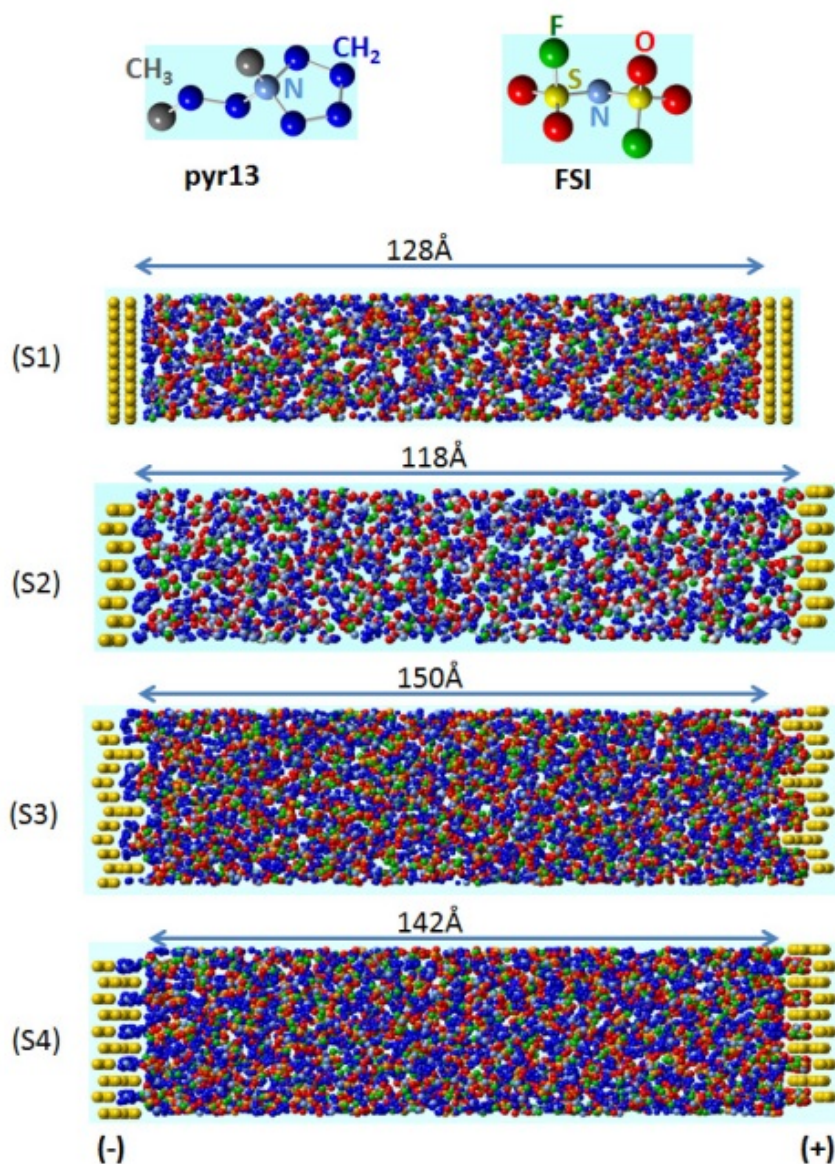


Figure 4.

Snapshots indicating the chemical structure of investigated electrolyte and the simulation setup for the systems studied in this work. The following electrode surface topography were studied: i) atomically flat basal graphite (S1), ii) the atomically corrugated prismatic graphite (S2), iii) a model of "weakly" corrugated surface (S3) where the widths of surface patterns were larger than the ionic diameter and iv) a model of "strongly" corrugated surface (S4) where the sizes of surface patterns matched the dimensions of electrolyte ions.

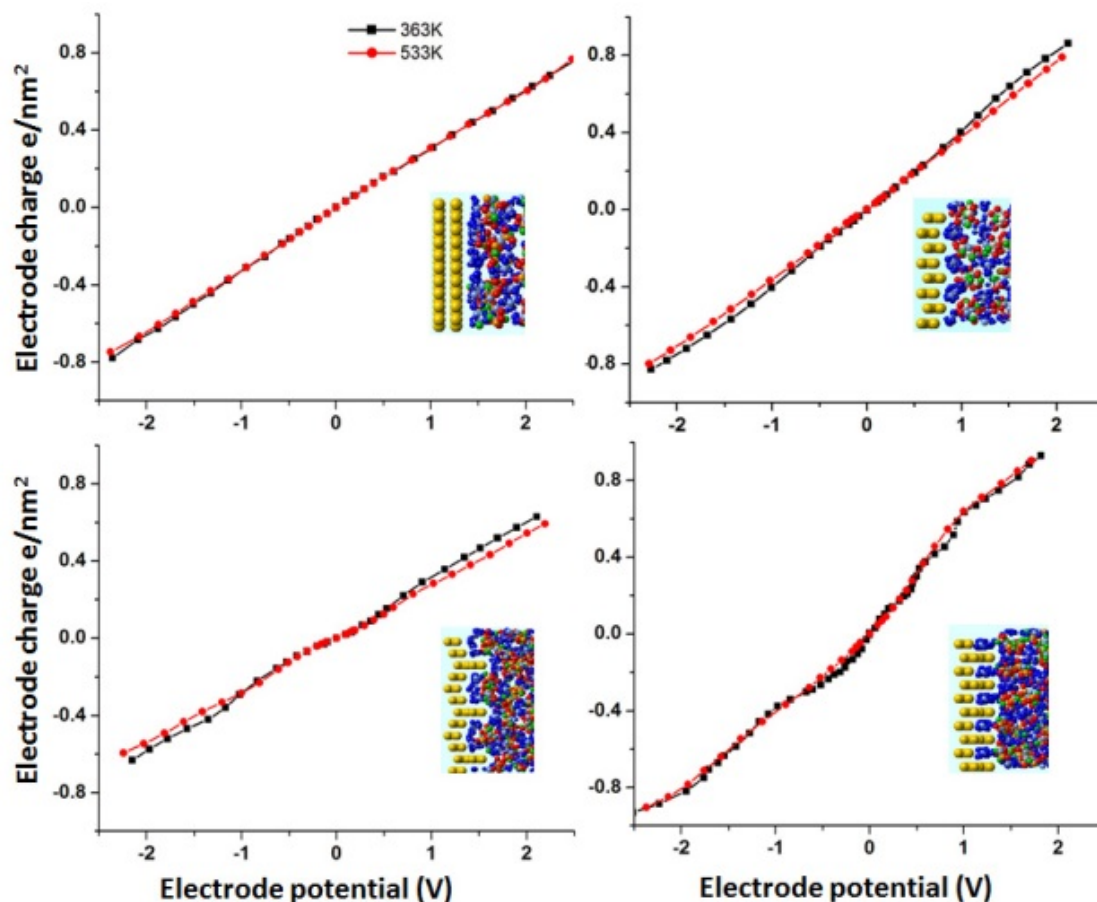


Figure 5.

The electrode charge density versus the electrode potential $\sigma=f(U)$ for the four surfaces studied at 363K (black lines) and 533K (red lines). The electrode surface topographies are indicated in plots as inserts. A more structured $\sigma=f(U)$ for surface S4 is consistent with larger variation in DC shown in main manuscript. Changing of temperature from 363K to 533K does not lead to significant changes in slopes of $\sigma=f(U)$ and therefore the integral capacities does not varies significantly in this temperature range. Overall we observe slightly smaller slopes at higher temperatures, which is consistent with a slight decrease of DC with temperature.

It should be noted that the total electrolyte charge density in the double layers near electrode are equal and opposite in sign to the electrode charge density. For the surface S4 (bottom-right panel) where an abnormal increase of DC with temperature was found at certain voltages we do not observe a large increase of the slope of $\sigma=f(U)$ for the highest temperature to suggest that a sharp release of electrolyte charge due to ion decoupling is responsible to the abnormal positive slope of DC vs. temperature. Instead the $\sigma=f(U)$ is more monotonic at 533K than at 363K.

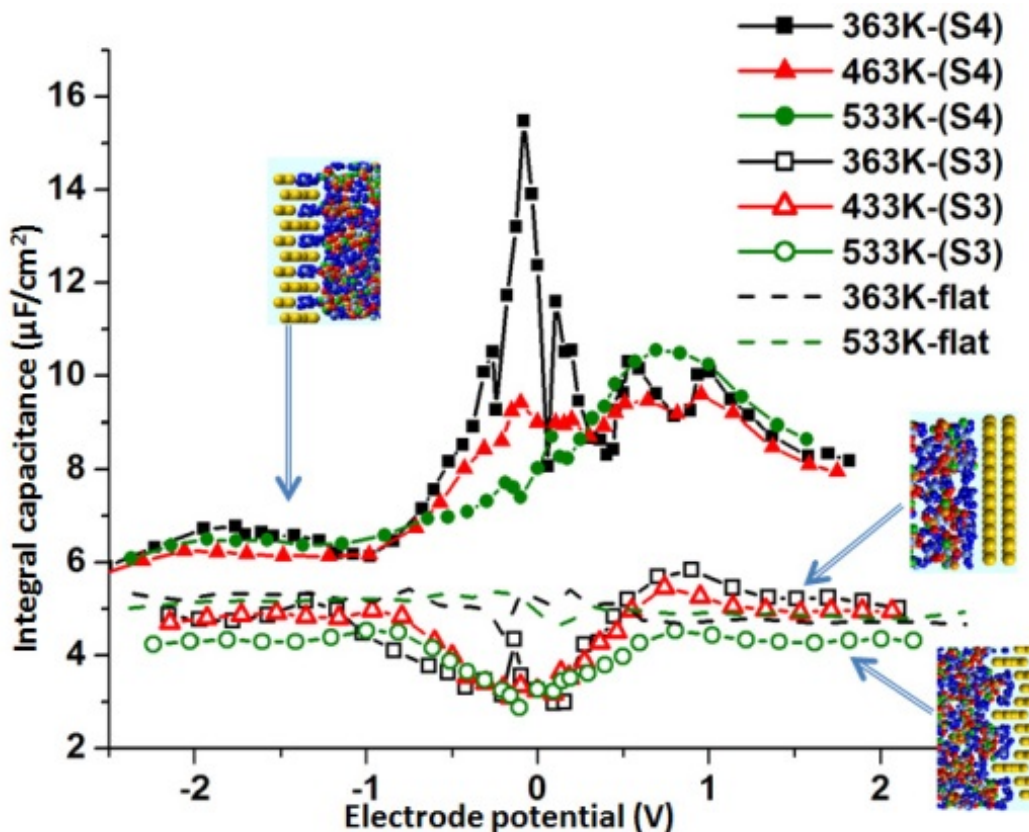


Figure 6.

The integral capacitance for three types of surfaces at several temperatures. It is interesting to note that IC for the surface S4 does change significantly with temperature only near PZC. However, above $\approx \pm 0.5\text{V}$ the IC does not change significantly with temperature, even for the most corrugated system S4. The ICs for the surface S3 is slightly lower than the IC near the flat surface. Note that the IC for prismatic surface (shown in the main manuscript) is larger than the IC for the flat surface but smaller than the IC for weakly rough surface S4. Therefore we notice here an oscillatory behavior of the value of IC as a function of the widths of surface patterns. Interestingly, oscillatory behavior of capacitance as a function of the widths was observed for slit pores.

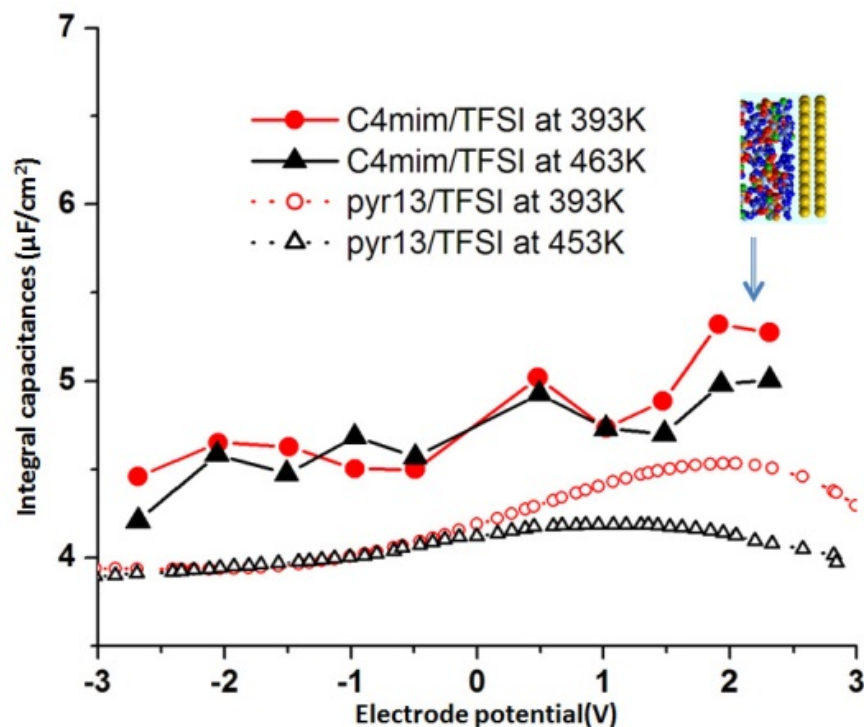


Figure 7.

The integral capacitance on flat surfaces for two different electrolytes, $[C_4MIM][TFSI]$ and $[pyr_{13}][TFSI]$ shows similar behavior (and magnitude) as $[pyr_{13}][FSI]$ on the flat surface. The IC varies between 4 to $5.5\mu F/cm^2$. The weak dependence of DC and ICs versus voltage and temperature on a flat electrode surfaces is confirmed for several additional electrolytes and it is likely a more general behavior. Note that sufficiently long simulations will eventually distinguish the features in DC predicted by Kornyshev model (i.e. an U-shaped at low voltages followed by two maxima and then decrease at higher voltages) however the variation of DC between minimum and maxima is rather small for flat electrodes (about $0.5\mu F/cm^2$).

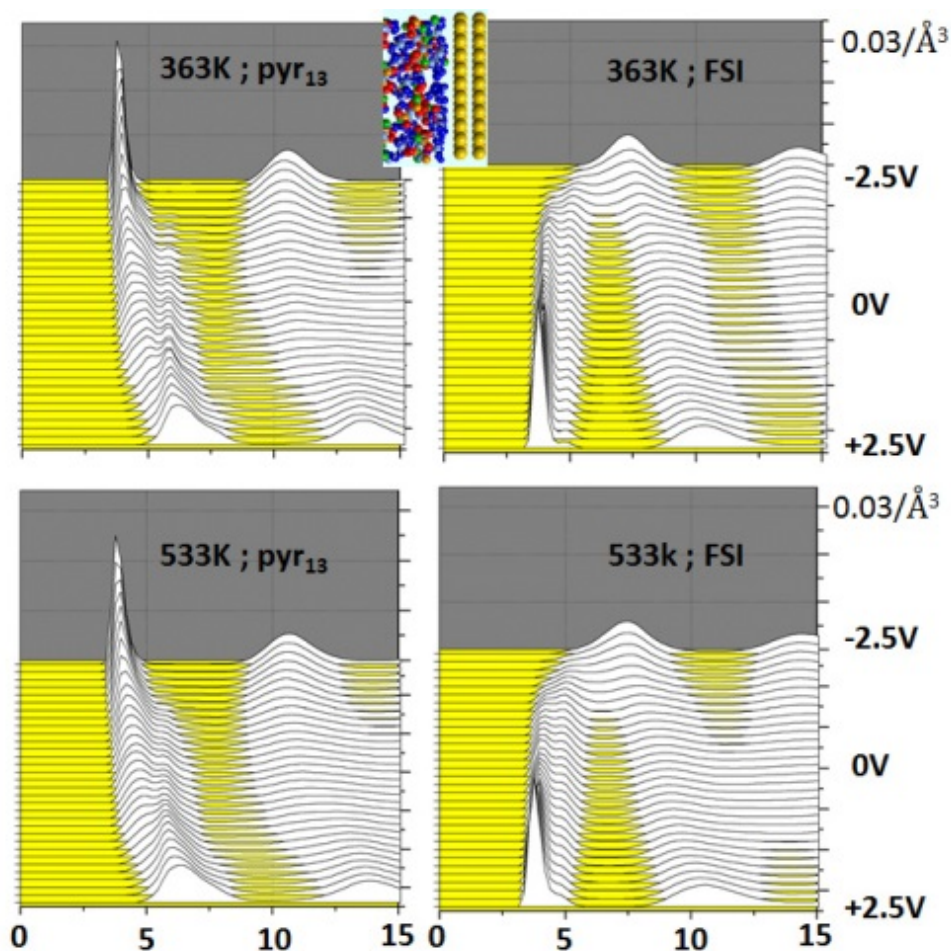


Figure 8.

Center of mass ionic density profiles as a function of electrode potential and distance from the electrode, for the flat surface at 363K and 533K. Represented in the x-axis of these plots is the distance from electrode. The zero along x-axes was defined as the position of the innermost graphene layer. Represented in the y-axes of these plots is the electrode potential. The z-axis represent the value of density from 0 to $0.03\text{ions}/\text{\AA}^3$. We observe a structuring of electrolyte in layers, with the counter-ions accumulating near the oppositely charged electrode followed by a layer of co-ions (as expected). The temperature increase from 363K to 533K does not generate large variations in these density profiles.

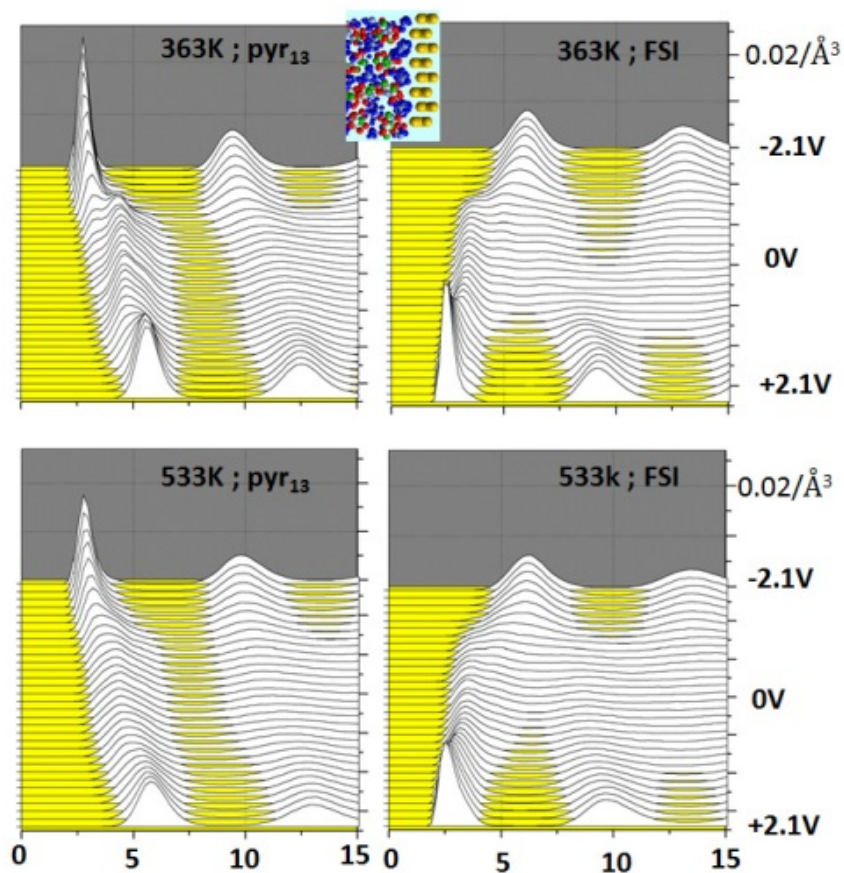


Figure 9.

The center of mass ionic density profiles as a function of electrode potential and distance from the electrode, for the prismatic surface (S2) at 363K and 533K. The position 0 along x-axes was chosen as the z-location of the innermost C atom. The increase of temperature slightly smooth out the overall dependence of density profile vs. potential and distance from electrode.

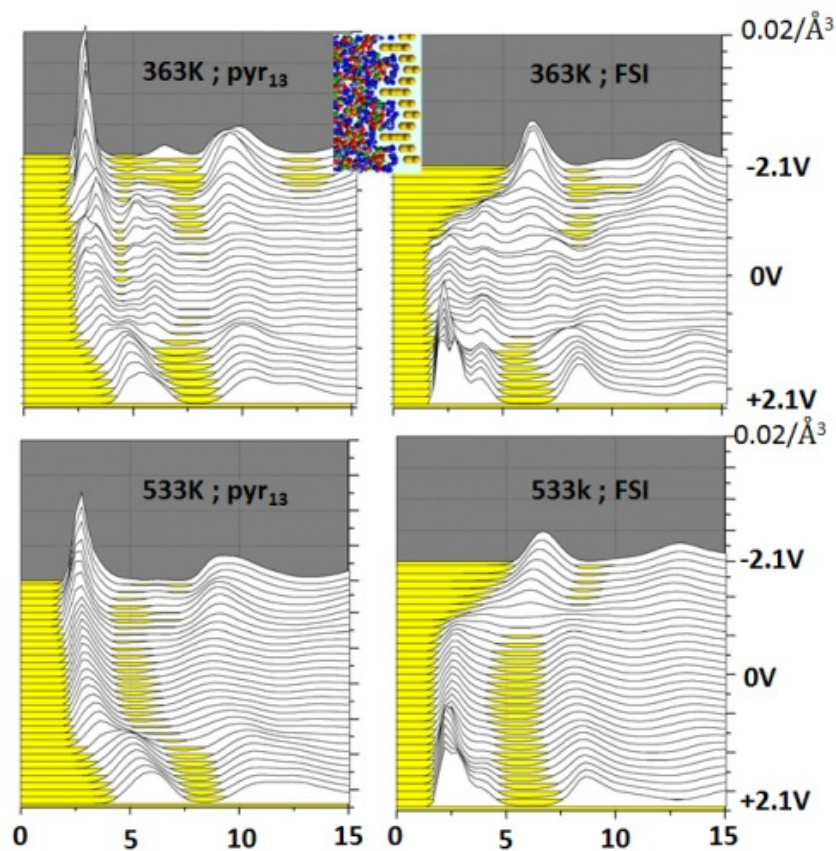


Figure 10.

The center of mass ionic density profiles as a function of electrode potential and distance from the electrode, for the corrugated surface (S3) at 363K and 533K. For this surface the lateral widths of the surface patterns is larger than the ion diameter and at least 2 layers of ions can be accommodated inside grooves. The zero along x-axis was chosen to be the location of the innermost C atom minus 5 Å.

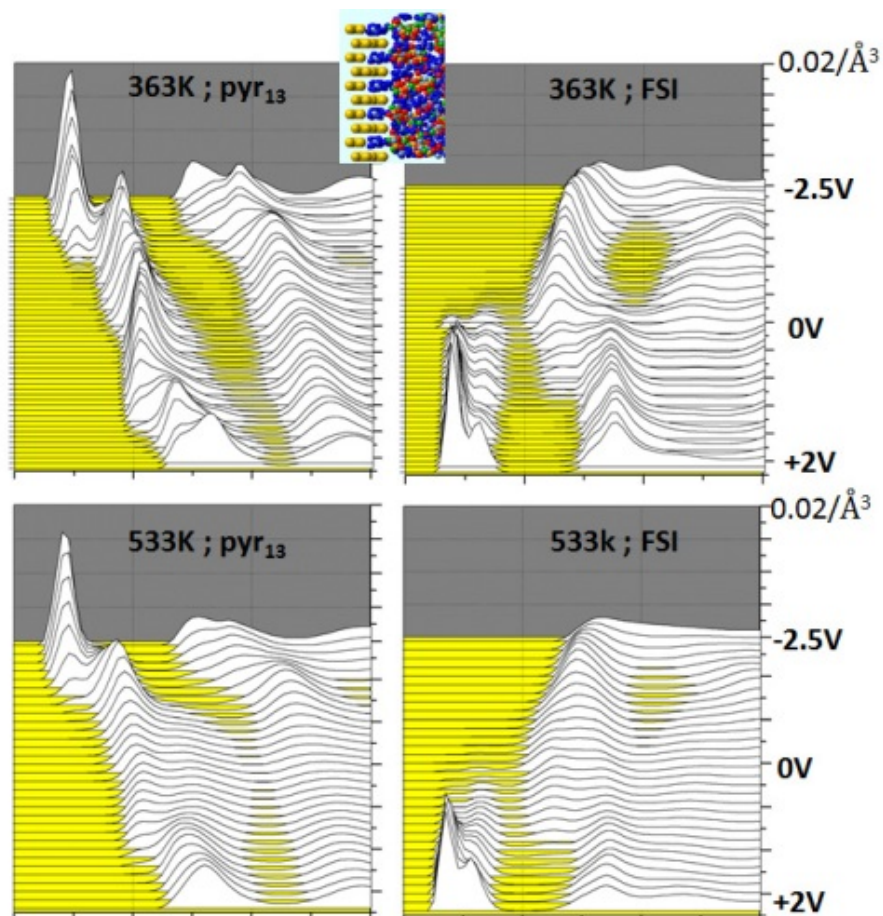


Figure 11.

The center of mass ionic density profiles as a function of electrode potential and distance from the electrode, for the highly corrugated surface (S4) at 363K and 533K. For this surface the lateral widths of the surface patterns is roughly equal with the ion diameter and only one single layer of ions can be accommodated in these tight grooves.

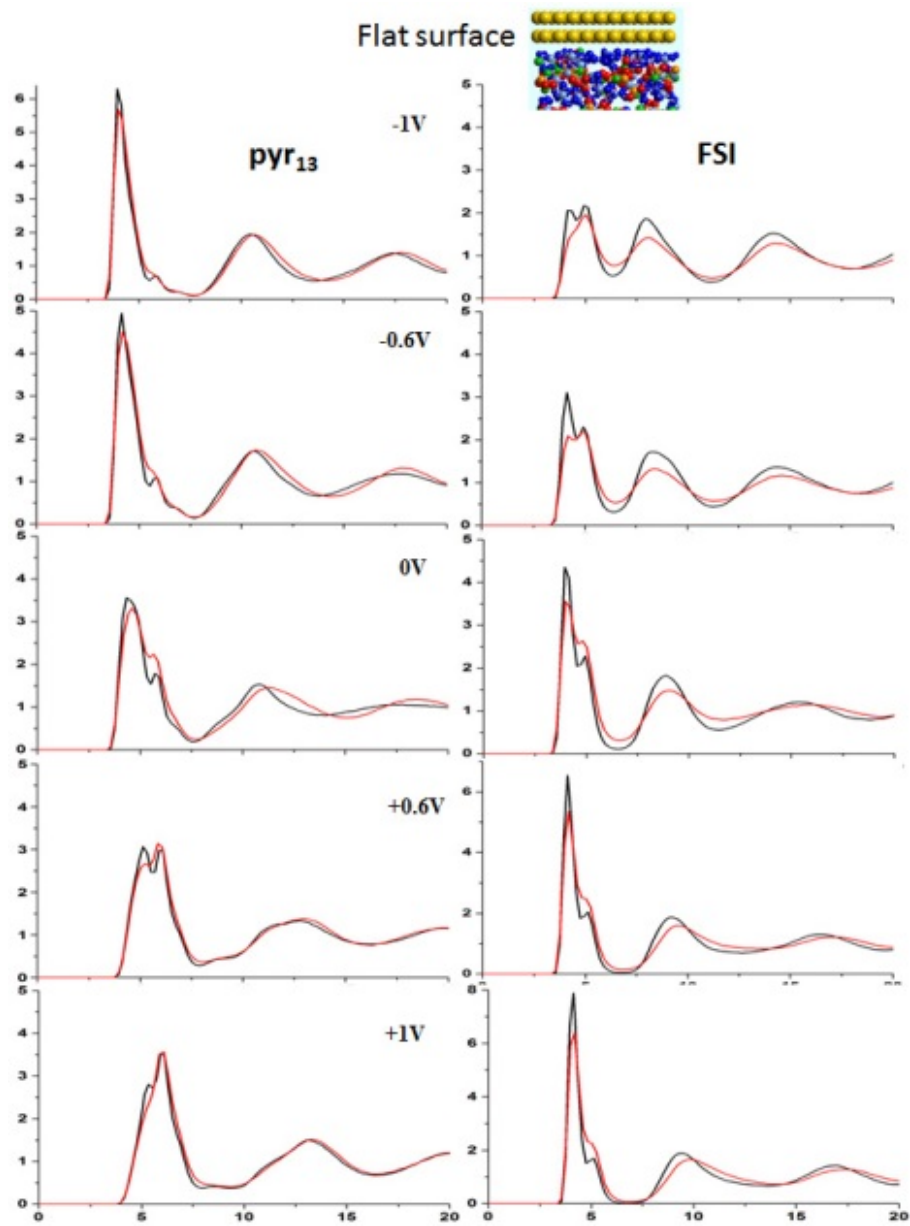


Figure 12.

The density profiles normalized to bulk density ($\rho(z)/\rho_{\text{bulk}}$) for ions on flat surface at several electrode potentials. The black and red lines represent the 363K and 533K respectively. For flat surface we observe very little impact of temperature on the interfacial structure.

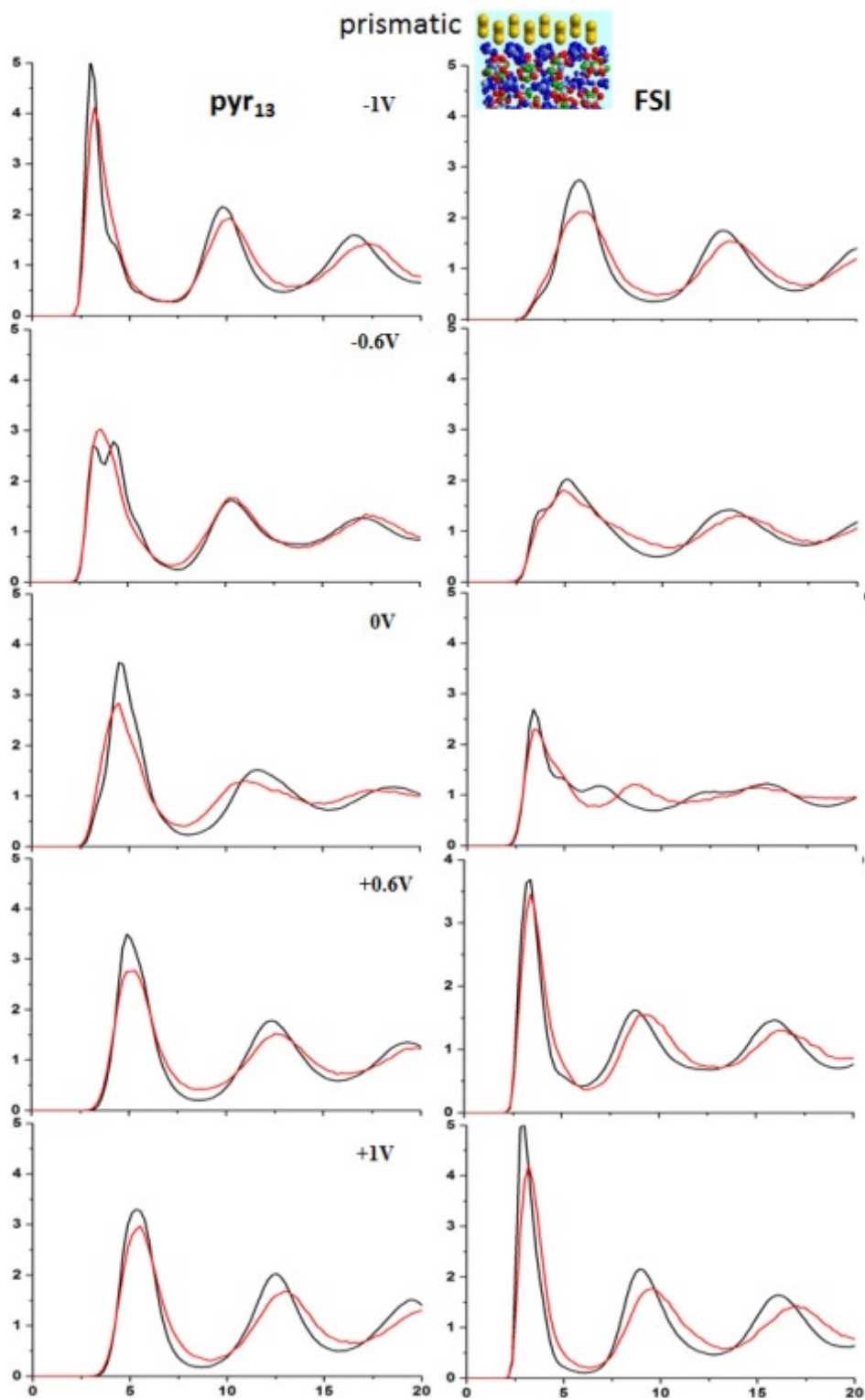


Figure 13.

The density profiles normalized to bulk density for ions on prismatic graphite surface at several electrode potentials. The black and red lines represent the 363K and 533K respectively.

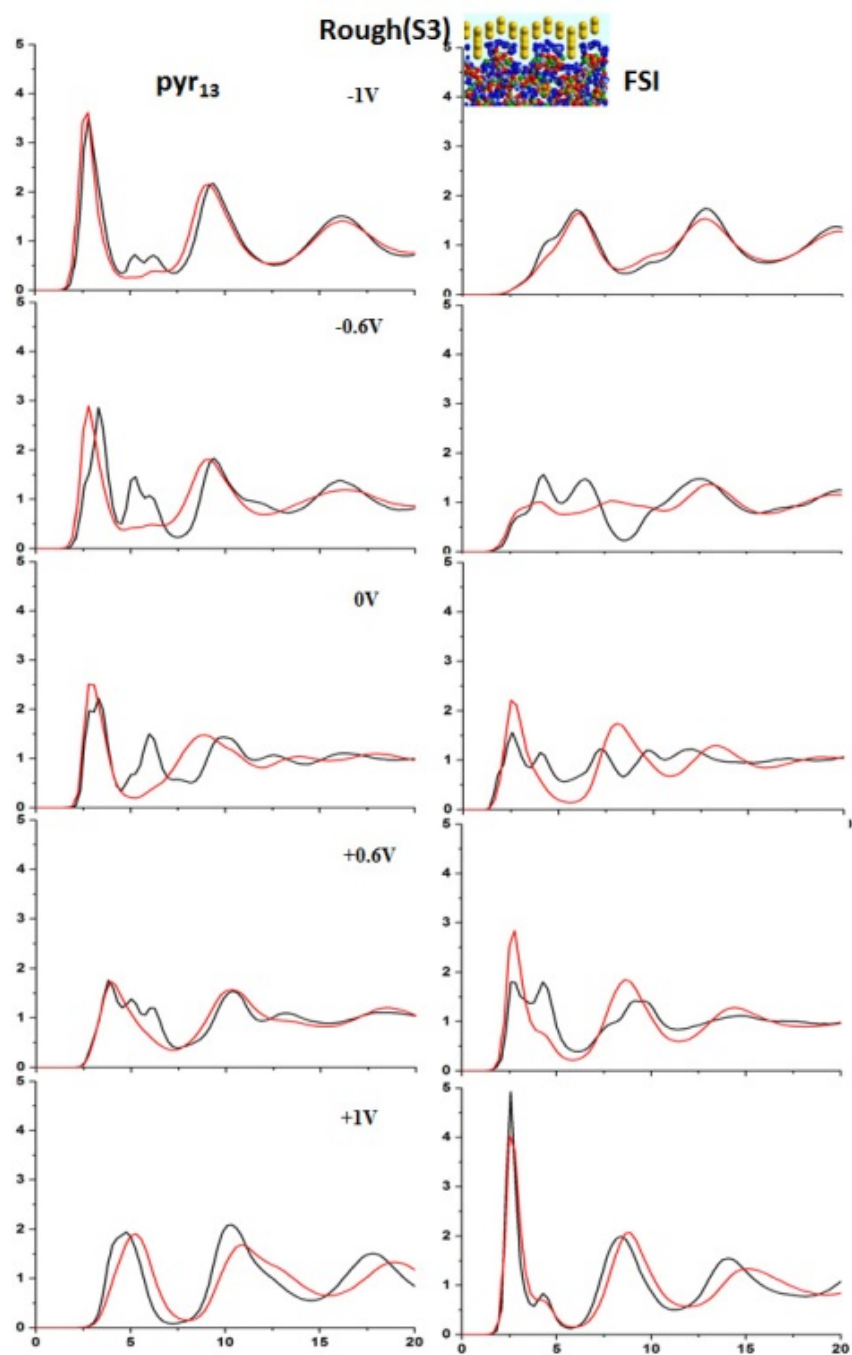


Figure 14.

The density profiles normalized to bulk density for ions on rough electrode surface (S4) at several electrode potentials. The black and red lines represent the 363K and 533K respectively.

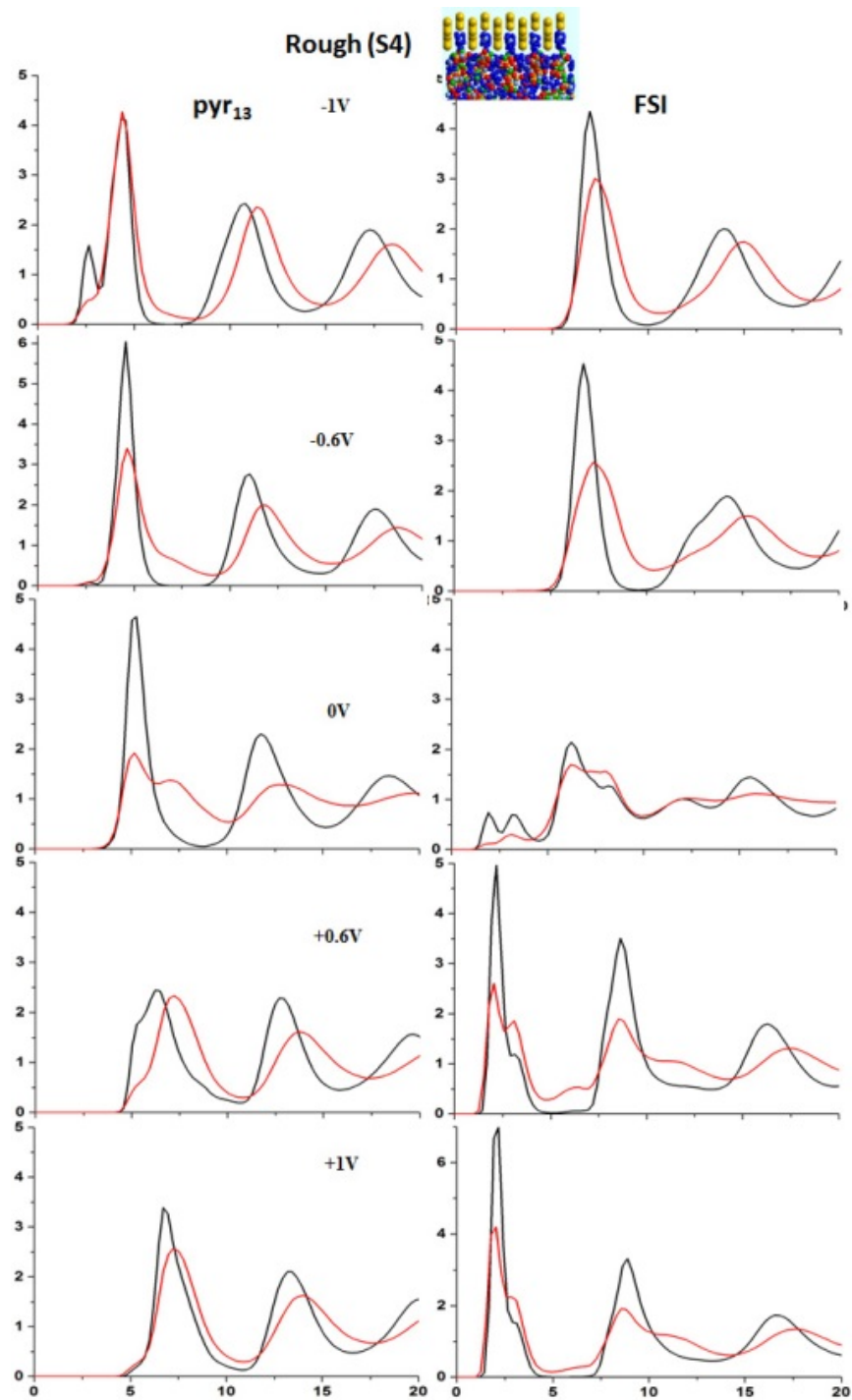


Figure 15.

The density profiles normalized to bulk density for ions on strongly corrugated surface (S4) at several electrode potentials. The black and red lines represent the 363K and 533K respectively. For this surface we observe large difference in interfacial structure with temperature increase, which is consistent with large differences in DC.

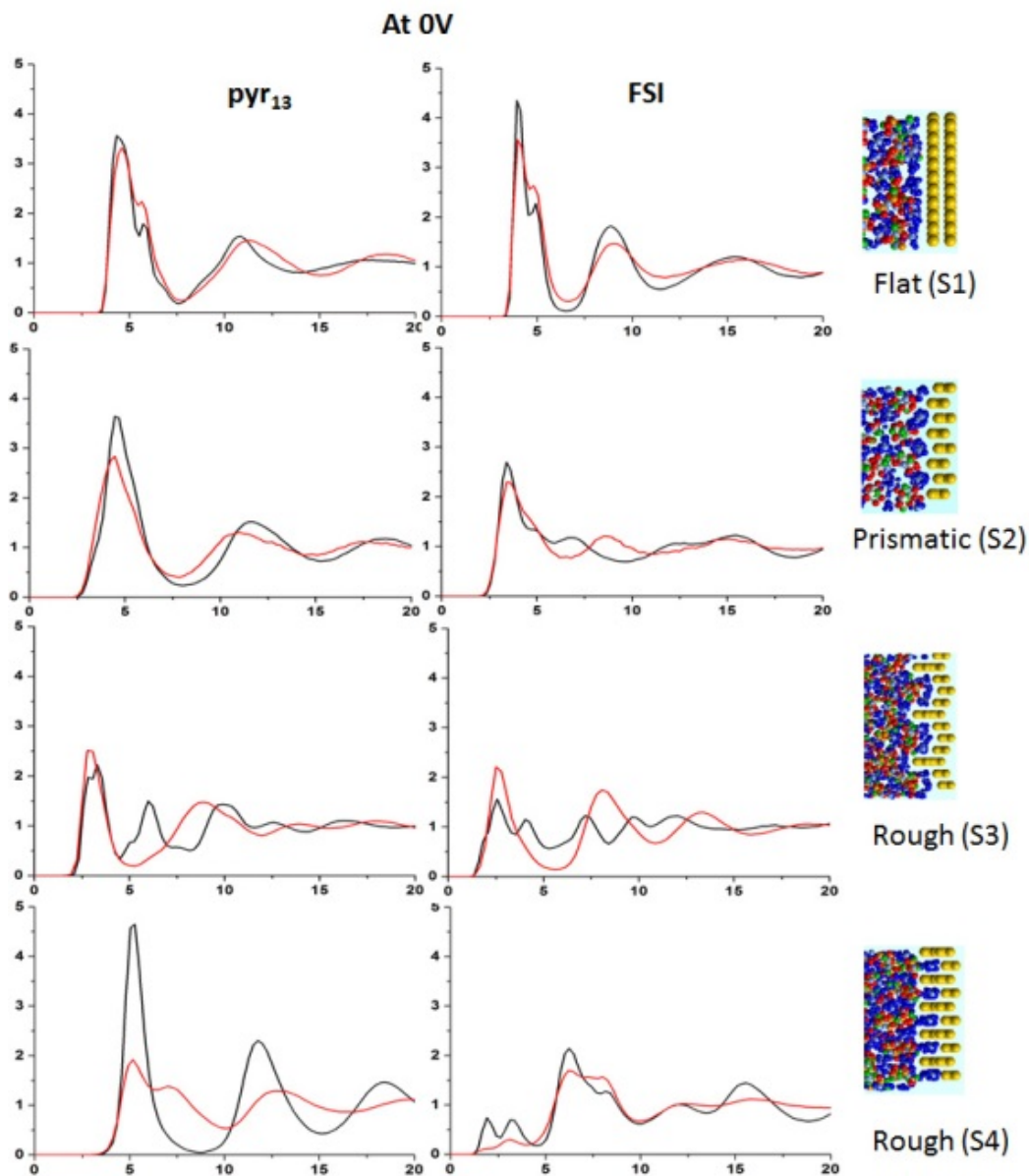


Figure 16.

The density profiles normalized to bulk density for ions at electrode potential of 0V, for several types of surface topography studied here. The black and red lines represent the 363K and 533K respectively. Clearly, the interfacial structure of the very rough surface S4 changes significantly temperature because of pyr₁₃ while the other surfaces modify their structure to a lesser extent.

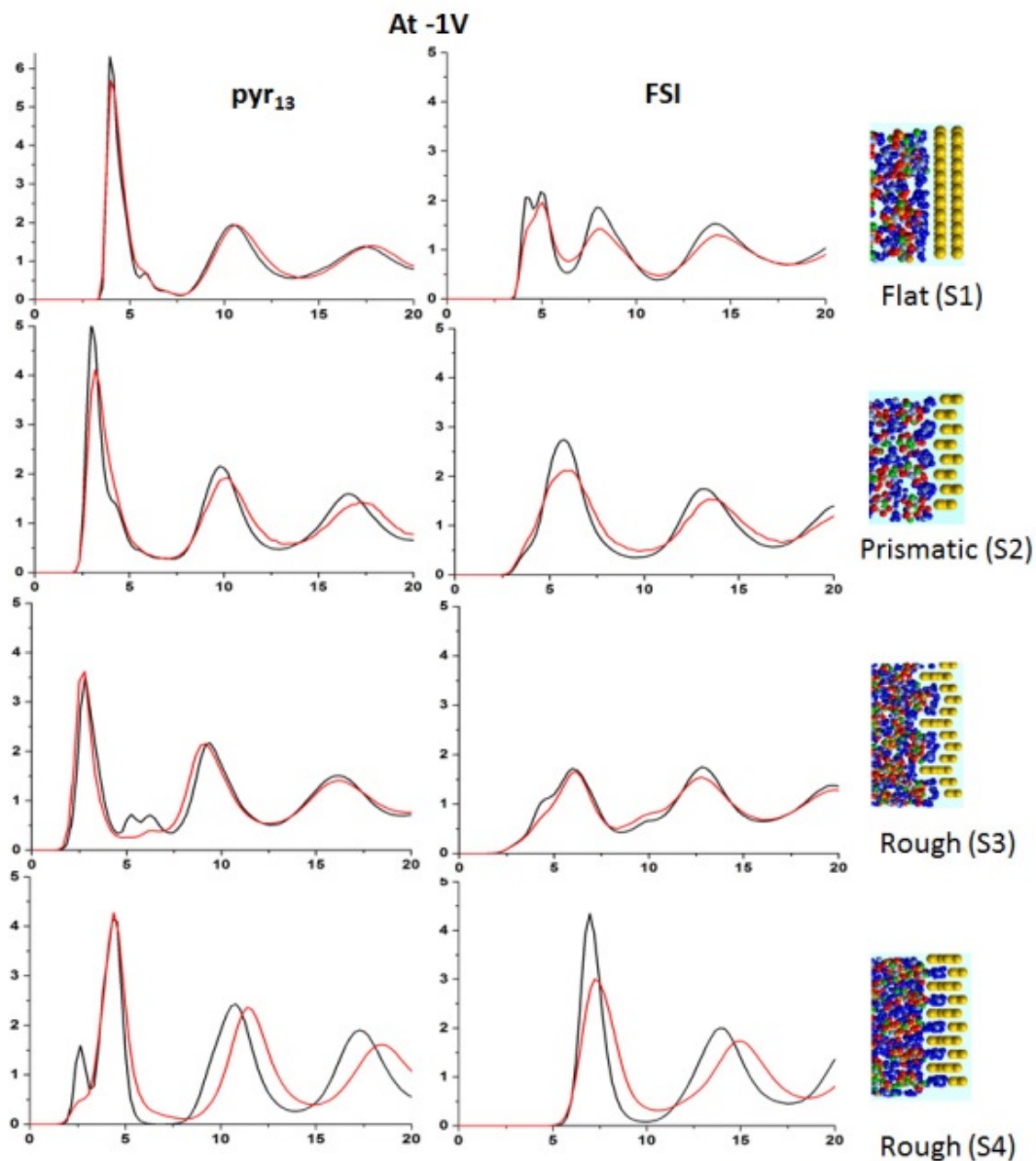


Figure 17.

The density profiles normalized to bulk density for ions at electrode potential of -1V, for several types of surface topography studied here. The black and red lines represent the 363K and 533K respectively. At higher voltages these density profiles became less dependent on temperature.

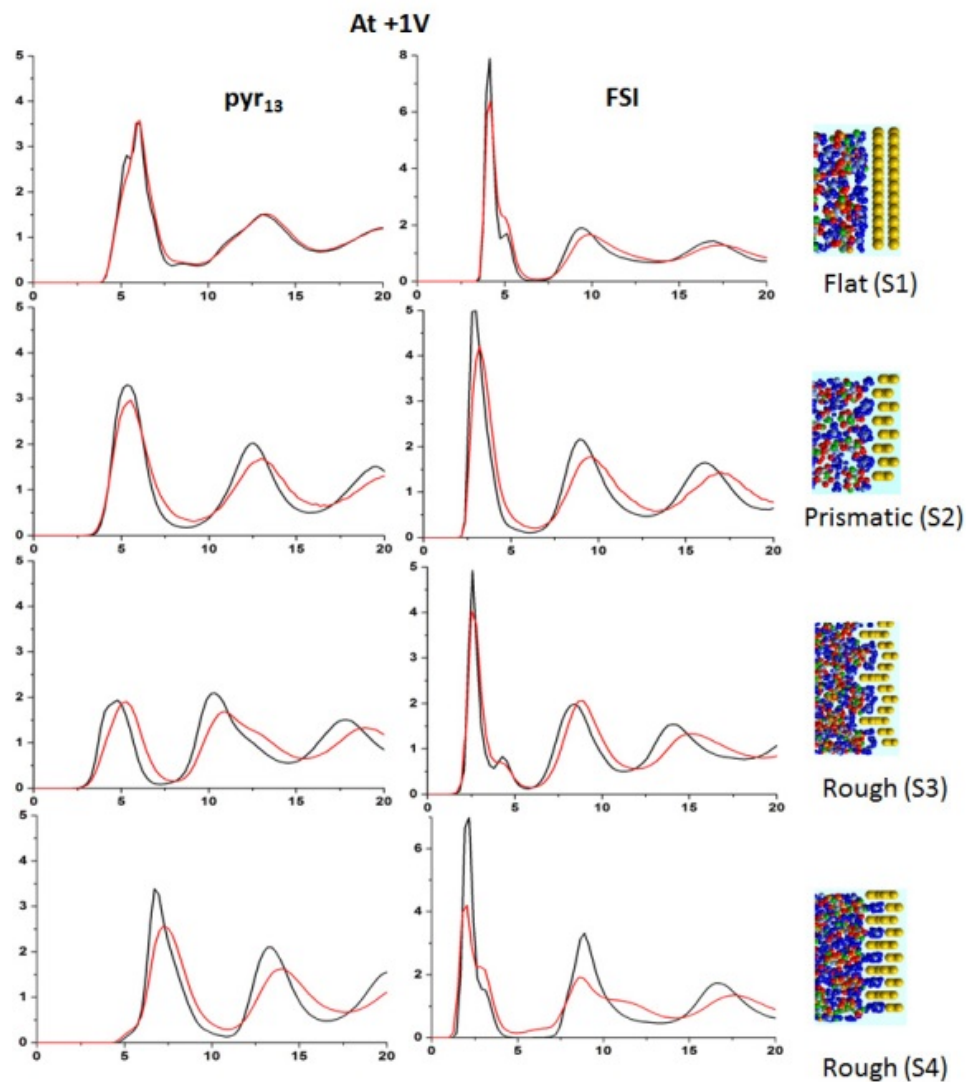


Figure 18.

The density profiles normalized to bulk density for ions at electrode potential of +1V, for several types of surface topography studied here. The black and red lines represent the 363K and 533K respectively. It is important to observe that at higher voltages the EDL structure is less affected by temperature increase than at lower voltages. Then we expect that the ICs at higher voltages (above $\approx 1V$) the values of ICs be less dependent on temperature and reflect the maximum possible packing in the interfacial layer. Note that for many common RTILs this translates in ICs of around $4-5\mu F/cm^2$.

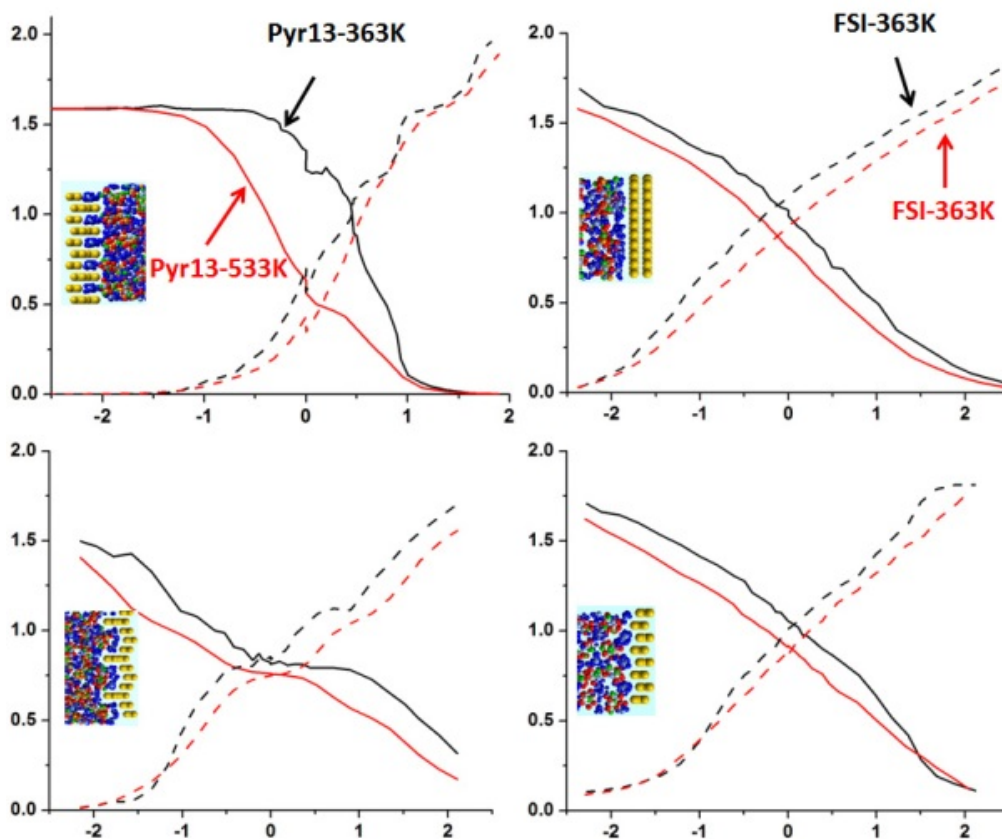


Figure 19.

The cumulative density profiles summed up over the first maximum in density profiles as a function of electrode potential. Note that the first maximum in the center of mass density profiles defines the ‘interfacial layer’ and it roughly extends to 5 Å width from the electrode position. These plots of cumulative densities are qualitative because the width of the interfacial layer cannot be defined precisely. However, we verified that slightly modifying the width over which the calculation of density was done leads to very similar qualitative behavior.

A systematic decrease of the interfacial density of ions with increasing temperature is observed which is consistent with an overall decrease of DC/IC with the temperature increase. The decrease of the interfacial density with temperature is caused by the slightly smaller bulk densities of electrolyte at higher temperature at atmospheric pressure and by a disordering of interfacial layer at higher temperature. Note that we do not observe at any voltage a sharp increase of counterion density at higher temperature which would explain the abnormal positive slope of DC vs temperature.

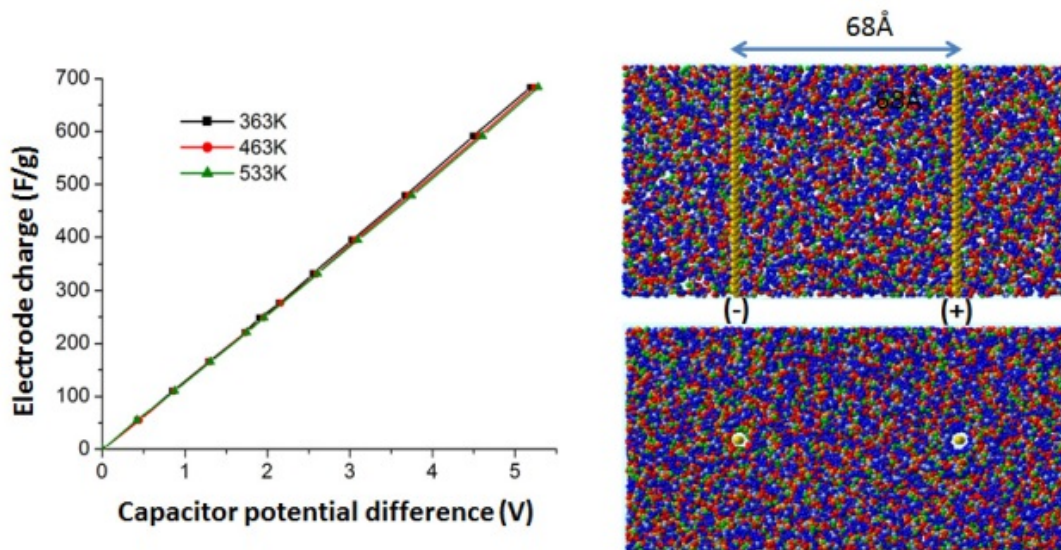


Figure 20.

In order to further investigate the impact of temperature on capacitance for various electrode geometries, we simulated a strongly curved electrode surface consisting of a single wire with atoms distributed as in all-trans $-C=C-C=C-$ immersed in electrolyte. The simulated systems consisted of two nanowires (one positively and the other negatively charged) immersed in electrolyte and separated at sufficiently large distance (more than 68\AA) to have the 2 electrodes decoupled. In this setup the double layers had cylindrical symmetry and therefore we can understand the impact of surface curvature on DC variation versus temperature. The dependence of electrode charge versus potential difference between the two wires (ΔU) is shown on the figure above. We observe a linear increase of charge versus potential consistent with capacities largely independent on voltage and only a slight decrease of the slope of $q=f(\Delta U)$ vs. temperature increase from 131.85 F/g at 363K to 128.95F/g at 533K . Therefore strongly curved EDL layers also generate only weakly changing capacities vs temperature. A qualitatively similar behavior was recently reported for larger curvature radius nanotubes by Feng et al.ⁱⁱⁱ

ⁱ Vatamanu, J., Borodin, O., Bedrov, D., Smith, G. D., *J. Phys. Chem. C*, **2012**, *116*, 7940–7951

ⁱⁱ Frenkel, D.; Smit, B. *Understanding Molecular Simulations: From Algorithms to Applications*; Academic Press: San Diego, CA, **2002**.

ⁱⁱⁱ G. Feng, S. Li, J. S. Atchison, V. Presser, P. T. Cummings, *J. Phys. Chem. C* 2013, **117**, 9178-9186.